SANDIA REPORT

SAND2001-1281
Unlimited Release
Printed May 2001

Direct Fabrication of Multi-Functional Nanocomposites via Supramolecular Self-Assembly

C. [illegible] Brinker, Hongyou Fan, Dhaval [illegible]shi, Mengcheng Lu, Nicola K. Husing, [illegible]g Lu, Kelly Simmons-Potter, B. G. Potter, Jr., and Alan J. Hurd

Prepared by
Sandia National Laboratories
Albuquerque, New Mexico 87185 and Livermore, California 94550

Sandia is a multiprogram laboratory operated by Sandia Corporation, a Lockheed Martin Company, for the United States Department of Energy under Contract DE-AC04-94AL85000.

Approved for public release; further dissemination unlimited.

Sandia National Laboratories

Issued by Sandia National Laboratories, operated for the United States Department of Energy by Sandia Corporation.

NOTICE: This report was prepared as an account of work sponsored by an agency of the United States Government. Neither the United States Government, nor any agency thereof, nor any of their employees, nor any of their contractors, subcontractors, or their employees, make any warranty, express or implied, or assume any legal liability or responsibility for the accuracy, completeness, or usefulness of any information, apparatus, product, or process disclosed, or represent that its use would not infringe privately owned rights. Reference herein to any specific commercial product, process, or service by trade name, trademark, manufacturer, or otherwise, does not necessarily constitute or imply its endorsement, recommendation, or favoring by the United States Government, any agency thereof, or any of their contractors or subcontractors. The views and opinions expressed herein do not necessarily state or reflect those of the United States Government, any agency thereof, or any of their contractors.

Printed in the United States of America. This report has been reproduced directly from the best available copy.

Available to DOE and DOE contractors from
U.S. Department of Energy
Office of Scientific and Technical Information
P.O. Box 62
Oak Ridge, TN 37831

Telephone: (865)576-8401
Facsimile: (865)576-5728
E-Mail: reports@adonis.osti.gov
Online ordering: http://www.doe.gov/bridge

Available to the public from
U.S. Department of Commerce
National Technical Information Service
5285 Port Royal Rd
Springfield, VA 22161

Telephone: (800)553-6847
Facsimile: (703)605-6900
E-Mail: orders@ntis.fedworld.gov
Online order: http://www.ntis.gov/ordering.htm

SAND2001-1281
Unlimited Release
Printed May 2001

Direct Fabrication of Multi-Functional Nanocomposites via Supramolecular Self-Assembly

C. Jeffrey Brinker* and Hongyou Fan
Catalytic & Porous Materials Department / SNL/UNM Advanced Materials Laboratory
Sandia National Laboratories, P. O. Box 5800, Albuquerque, NM 87185

Dhaval A. Doshi and Mengcheng Lu
Department of Chemical & Nuclear Engineering / SNL/UNM Advanced Materials Laboratory
University of New Mexico, Albuquerque, NM 87106

Nicola K. Husing
Institute of Inorganic Chemistry, Vienna University of Technology
Vienna, Austria

Yunfeng Lu
Department of Chemical Engineering
Tulane University, New Orleans, LA 70005

Kelly Simmons- Potter
Laser Optics and Remote Sensing Department / Sandia National Laboratories

B. G. Potter Jr
Electronic and Optical Materials Department / Sandia National Laboratories

Alan J. Hurd
Manual Lujan Center / Los Alamos National Laboratory
Los Alamos, NM 87545

Abstract follows

* Author to whom correspondence should be addressed: cjbrink@sandia.gov

Abstract

The ability to efficiently organize molecular components at the nanometer scale will greatly influence the future of advanced materials in applications for electronics, catalysis, photonics, and sensors and their integration into micro-systems. This stems from the fact that interplay of structure, organization and dynamics at the molecular level are all vital in determining a functional response. Based on this premise, we have successfully developed efficient, continuous processes to form ordered nanocomposite materials via evaporation induced self-assembly (EISA). Here, we describe the combination of silica-surfactant self-assembly with simple patterning strategies to yield functional, organized porous thin films that may be important for a number of technological applications including sensor arrays, optics, and microfluidic devices.

Acknowledgments

The authors would like to thank C. Braunbarth for discussions about the phase transformation. We also thank R. Assink for assistance with NMR experiments, Y. Guo for assistance with TEM, and C. Ashley for compiling and editing this report. This work was partially supported by SNL's Laboratory Directed R&D program, the UNM/NSF Center for Micro-Engineered Materials, FWF Austria, and the DOE Basic Energy Sciences Program.

Contents

Figures

Tables

Introduction

The ability to pattern porous thin films is important for a number of technological applications including sensor arrays, optics, and microfluidic devices. Mesoporous silicas [1] are attractive for such applications because they have internal connectivity and variable density that can be tailored by preparative conditions. Soft lithographic approaches[2] have been used to pattern mesoporous films but require long processing times[3, 4] or have been limited to defining physically the presence or absence of discrete isolated regions[3, 4]. Rapid patterning of organofunctionalized mesoporous thin films via pen lithography, ink-jet printing, and selective dewetting has also been demonstrated recently[5], but to-date no one has successfully patterned thin-film mesostructure or properties. This report documents our efforts to control the mesostructured of thin films and demonstrates our ability to optically define and continuously control both structure and function on the macro- and mesoscale.

Methods and Procedure

Precursor solutions were prepared by addition of the surfactant (Brij 56, $C_{16}H_{33}(OCH_2CH_2)_{10}OH$, Aldrich) and the PAG (a diaryliodonium hexafluoroantimonate salt, Sartomer) to polymeric silica sols made by a two-step procedure (A2**). This procedure was designed to minimize the siloxane condensation rate and foster facile silica-surfactant supra-molecular self-assembly during film deposition. First, TEOS ($Si(OC_2H_5)_4$), ethanol (C_2H_5OH), water and HCl (mole ratios 1:4:1:5 x 10^{-5}) were heated at 60 °C for 90 min. This sol was diluted on volume basis with ethanol (1 sol : 2 C_2H_5OH) followed by addition of water and HCl. Finally, Brij 56 and PAG were added such that the final reactant mole ratios were 1 TEOS : 20 C_2H_5OH : 3.1 H_2O : 0.0065 HCl : 0.063-0.127 Brij 56 : 0.0156 PAG. Alternatively, film such as those depicted in Fig. 1, scheme 2 were made using lower ethanol content and methyltriethoxysilane (MTES) to obtain thick crack free films. The molar ratio used was 1 TEOS : 1 MTES : 3.8 C_2H_5OH : 7 H_2O : 0.01 HCl : 0.096 Brij 56 : 0.014 PAG.

Films were deposited on (100)-silicon by dip-coating at 25.4 cm/min. Within 30 to 60 min. of deposition, the samples were irradiated at 256 nm for times ranging from 15 s to 2 h through a mask via proximity printing to effectively transfer the pattern onto the silica thin film. Etching of the films was performed using a 0.2 M aqueous NaOH solution for a period of 5 to 10s. Calcination treatments to promote continued siloxane condensation and remove surfactant templates and residual organics associated with PAG were conducted in air at 450 °C for 3 hours using a ramp rate of 1°C/min. HCl exposures of unirradiated films were performed by placement in a chamber containing dispersed droplets of concentrated HCl for 2 hr.

Magic angle spinning ^{29}Si nuclear magnetic resonance indicates an extent of condensation of 82.1% ($Q^2/Q^3/Q^4$ =8.22/55.08/36.7) for irradiated, powdered films (2hr UV exposure) compared to 80.8% ($Q^2/Q^3/Q^4$ =9.61/57.75/32.64) for the corresponding unirradiated samples. The superscript "i" in Q^i represents the number of bridging oxygen atoms surrounding the central silicon atom. It can be expected that this difference is much greater immediately after irradiation, but lengthy acquisition times (16h) needed to perform the NMR experiment preclude our acquisition of data at '$t = 0$' and allow continued siloxane condensation to occur, diminishing this difference.

Results and Discussion

Here we report patterning of the mesostructure within a thin film. Our procedure uses evaporation-induced self-assembly to prepare a photosensitive thin-film mesophase containing a photoacid generator (PAG). We then exploit the pH-sensitivity of both the siloxane condensation rate and the silica-surfactant self-assembly process to define optically film location, mesostructure, and properties. The procedure begins with a homogeneous solution of silica, surfactant, photoacid generator (PAG, a diaryliodonium salt) and HCl with initial acid concentration designed to minimize the siloxane condensation rate [6, 7]. Preferential ethanol evaporation during dip- or spin-coating concentrates the depositing solution in water and non-volatile constituents, thereby promoting self-assembly [8, 9] into a photosensitive, one-dimensional hexagonal (1-dH) silica/surfactant mesophase. Because it bears a long-chain hydrocarbon, the PAG serves as a co-surfactant during the assembly process, which promotes its uniform incorporation within the mesostructured channels of the 1-dH film.

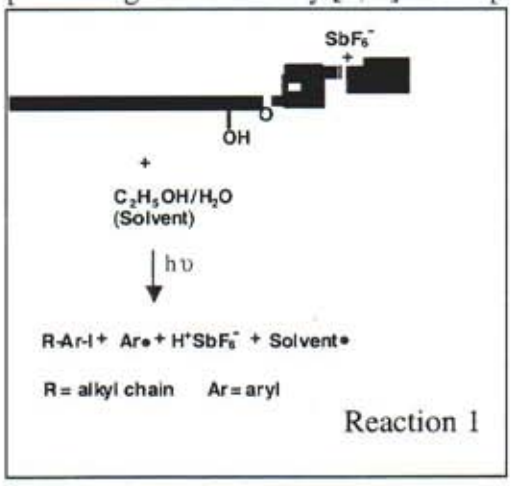

Reaction 1

Irradiation of the PAG at a maximum wavelength (λ_{max}) of 256 nm (reaction 1) results in homolytic or heterolytic photodecomposition to yield the Brønsted super-acid, $H^+SbF_6^-$, plus an iodoaromatic compound and organic by-products [10]. Thus ultraviolet (UV) exposure of the photosensitive mesophase through a mask creates patterned regions of differing acid concentrations compartmentalized within the silica mesophase (Fig. 1). Co-incorporation of a pH-sensitive dye (ethyl violet) allows direct imaging of these patterned regions as in Fig. 2A, where the yellow (exposed) and blue (masked) regions correspond to pH 0 and pH 2, respectively[1].

[1] In aqueous solution, ethyl violet is violet-blue for pH ≥ 2 and yellow for pH < 0.

Suppression of the siloxane condensation rate during film deposition enables several modes of optically mediated patterning. Because acid generation promotes

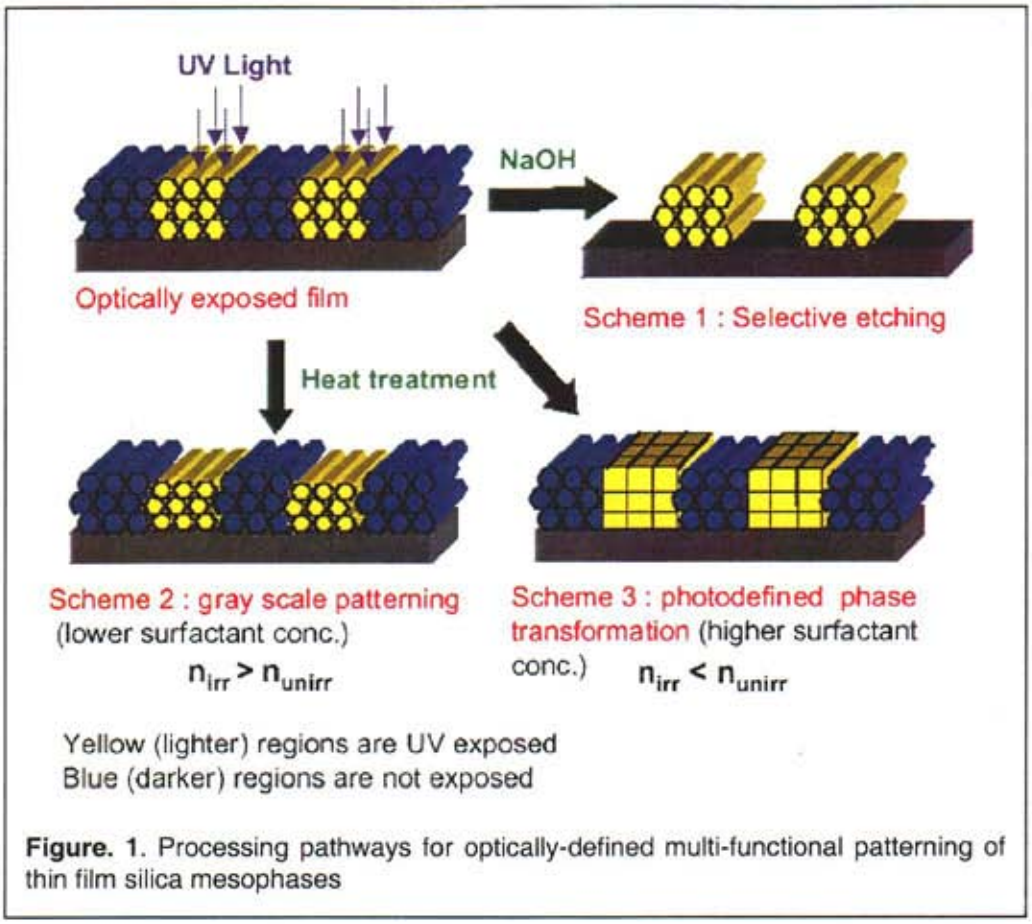

Figure. 1. Processing pathways for optically-defined multi-functional patterning of thin film silica mesophases

siloxane condensation, selective UV exposure results in patterned regions of more and less highly condensed silica. Differential extents of siloxane condensation result in turn in differential solubility, allowing selective etching of more weakly condensed regions in aqueous base (0.2 M NaOH) (Fig. 1, scheme 1). An optical micrograph of a UV-exposed and etched thin-film mesophase after calcination to remove the surfactant templates (Fig. 2B) reveals that the film is present only in the exposed regions. The plan-view transmission electron microscopy (TEM) image (Fig. 2B inset) reveals a striped mesoscopic structure consistent with a 1-dH mesophase with unit cell size $a = 37$ Å. We have also used a C_3F_8 plasma to directly etch the unexposed regions of photopatterned films[2]. This process could potentially eliminate the need for a photoresist in the patterning of mesoporous low dielectric constant films needed by the microelectronics industry [11].

[2] An etching resolution of 1 μm was demonstrated with a C_3F_8 plasma etching procedure (D.A. Doshi, M.J. Barela, C.J. Schwarz, unpublished results).

Organic by-products of the (patterned) PAG photodecomposition process render UV-exposed regions of the film hydrophobic (contact angle = 40°) relative to adjoining unexposed regions (contact angle <10°). This differential wetting behavior is evident in

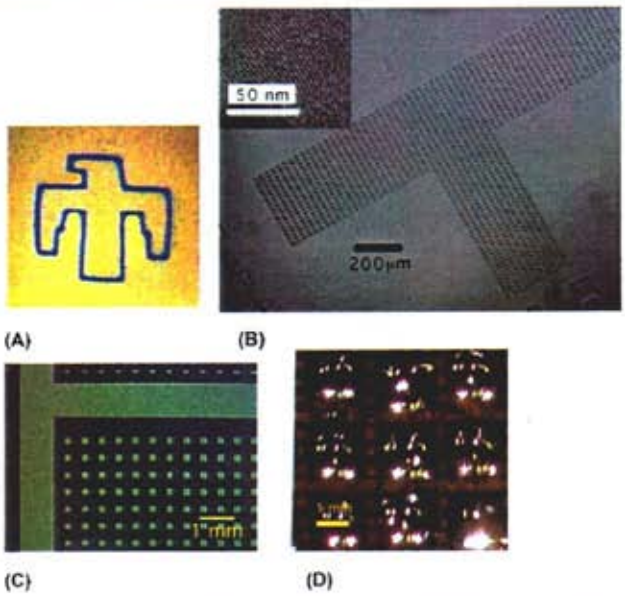

Figure. 2. Optical patterning of function/properties in thin-film silica mesophases. (**A**) Optical image of localized acid generation via co-incorporation of a pH-sensitive dye (ethyl violet). The blue areas observed for the unexposed film correspond to $pH^* \geq 2.0$ and the yellow areas observed for the exposed film to $pH^* \sim 0$ (where pH^* refers to the equivalent aqueous solution pH required to achieve the same colors) (**B**) Optical micrograph of a UV-exposed and selectively etched mesostructured thin film (after calcination). Feature size ≈ 10 μm. Inset : TEM image of the film seen in (**B**) consistent with the [110]-orientation of a 1-dH mesophase with lattice constant a = 37 Å. (**C**) Optical interference image showing thickness and refractive index contrast in a patterned, calcined film. The green areas correspond to UV-exposed and calcined regions and the black areas to unexposed and calcined regions. (**D**) Optical image of an array of water droplets contained within patterned hydrophilic-hydrophobic corrals. Water droplets sit on hydrophilic regions with contact angle <10° and are bounded by the hydrophobic UV-exposed regions with contact angle = 40°.

Fig. 2D where a patterned, square, hydrophilic lattice serves to corral water into an array of monosized droplets. Such corrals can be used to selectively derivatize hydrophilic regions with aqueous-based reagents and/or biomolecules. Preliminary work using aqueous solutions of metal salts has demonstrated paterning of Ni and Co oxides into optically defined periodic arrays within thin-film silica mesophases.

A second aspect of our approach is the optical definition of film mesostructure and associated structure-related properties like pore size, pore connectivity and refractive index (Fig 2C). Depending principally on the type and concentration of surfactant, we realize two contrasting types of behavior. As depicted in Fig. 1, if we heat the patterned film, we obtain adjoining regions of differing refractive index where the sign of the refractive index contrast Δn may be either positive ($n_{irradiated} > n_{unirradiated}$) or negative. Both types of behavior result from a greater extent of siloxane condensation in the UV-

exposed regions. For positive Δn , the UV-exposed regions are still hexagonal but denser than unexposed regions. We used a cantilever beam technique[12, 13] to measure the development of condensation-induced, thin-film biaxial tensile stress and found that the differing extent of siloxane condensation was UV-dose dependent. Therefore by spatially

	As-prepared films		Calcined films	
	t (nm)	*n*	*t* (nm)	*n*
Unirradiated	365.1 ± 2.6	1.454 ± 0.001	229.3 ± 2.2	1.302 ± 0.002
UV-irradiated	360.2 ± 2.1	1.457 ± 0.001	239.9 ± 2.3	1.277 ± 0.002

Table 2 : Ellipsometry data showing thickness (t) and refractive index (n) (at λ= 630nm) for films exhibiting 1dH to tetragonal phase transformation

varying the UV exposure using grayscale lithography we can pattern continuous

Exposure (min)	Thickness (nm)	n	d_{100} (Å)	Unit Cell (Å)	Porosity[a]	Pore Size[b] (Å)	Pore Volume[a] (cc/g)	Surface Area[a] (m^2/g)
0	192.5	1.318	44.58	51.44	57.1%[c]	20.5[c]	0.46[c]	897[c]
1	190.3	1.330	42.90	49.50	50.5 %	19.0	0.38	813
2	189.4	1.333	41.85	48.29	47.3%	18.5	0.34	736
3	184.7	1.359	39.90	46.04	39.3%	17.9	0.24	548

[a] by surface acoustic wave (SAW) based N_2 adsorption technique. Calcination temperature was reduced to 425 °C for compatibility with SAW substrates. [b] Pore size = 4V/A. [c] extrapolated

Table 1 : Properties of films resulting from differing UV exposures times followed by calcination at 425 °C

variations in the film refractive index and thickness, as well as structural properties of the 1-dH thin film mesophase (Table 1).

We have used our ability to pattern refractive index, as evinced by the optical interference image shown in Fig 2C, to create optical diffraction gratings[3]. Exposure of a photosensitive film with an excimer laser (λ=248 nm) through a phase mask resulted in a 543 nm grating structure [14] with Δn ~ 0.025 (Fig. 1, scheme 2) after calcination to remove the surfactant templates. The measured Littrow angle of 34° is consistent with the mask period of 564 nm. Compared to gratings patterned in glass [15, 16] or liquid crystals [17], the ordered porosity of our gratings allows the diffracted intensity to be tunable by and sensitive to certain absorbing molecules in the environment.

Using a higher initial surfactant concentration, near that required for the 1-dH to cubic transformation without added acid, we observe a negative refractive index contrast that results from a hexagonal-to-tetragonal mesophase transformation (Table 2).

Evidence for the optically defined phase transformation was obtained by X-ray diffraction (XRD) and TEM. After calcination at 450°C to remove surfactant, the XRD

[3] See supplementary information in Appendix A

pattern of the unirradiated film (Fig. 3, trace A) is consistent with a 1-dH mesophase with lattice constant $a = 42.1$ Å, whereas the pattern of the irradiated sample (Fig. 3 trace B) is assigned to a tetragonal (distorted cubic) mesophase with $a = 66.8$ Å and $b = c = 72.8$ Å[4] along with residual traces of the untransformed parent structure[5]. The XRD pattern of an unirradiated PAG-containing film exposed to HCl vapor prior to calcination is comparable to that of the irradiated sample but shifted to a higher d-spacing (Fig. 3, trace C). The cross-sectional TEM image of the unirradiated film (Fig. 4A) reveals a striped pattern characteristic of the [110]-orientation of a 1-dH mesophase ($a = 42.7$ Å), with mesopore channels oriented parallel to the substrate surface; that for the irradiated film (Fig. 4B) exhibits predominantly a diamond-shaped texture consistent with the [010]-orientation of a tetragonal mesophase[6]. The topotactic relationship between the 1-dH and tetragonal mesophases (Fig. 4, insets) indicates that the transformation results in a factor of $\sqrt{3}$ increase in lattice constant.

The mechanism of this phase transformation may be understood by considering how silica/surfactant mesophases reorganize in response to increased extents of siloxane condensation. The thermodynamically favored phase is that which allows the surfactant headgroup area a to be closest to its optimal value a_o, while maintaining favorable packing of the hydrophobic surfactant tails [18, 19]. The influence of a_o along with the surfactant volume v and tail length l on the resultant mesophase can be understood qualitatively by the dimensionless packing parameter $g = v/a_o l$: where $g = 1$ favors formation of vesicles, bilayers, or lamellar mesophases and decreasing values of g result in the formation of progressively higher curvature mesophases and ultimately spherical micelles ($g < 1/3$) [18, 19]. Monnier et al. [20] introduced the term G_{inter} in their free energy expression to account for electrostatic interactions between the silica framework and surfactant head groups. When the framework charge density matches the average surface charge density of the surfactant head groups $1/a$, G_{inter} is minimized, establishing a_o, which in turn influences g and the mesophase curvature.

---

[4] We define the co-ordinate system to maintain the c direction parallel to the cylinder axes of the as-deposited hexagonal mesophase. The two in-plane directions (b and c) experience a constraint to shrinkage, whereas the a direction normal to the substrate is unconstrained and hence free to shrink, resulting in the smallest lattice constant. For the transformed mesophase the lattice constant c is determined from TEM (Fig 4B). Using c to solve the d_{111} spacing in the XRD pattern (Fig 3, trace B) we find $b=c$.

[5] The (200) and (400) reflections of the tetragonal phase can also be indexed as the (100) and (200) reflections of the untransformed parent 1-dH mesophase.

[6] The occasional presence of horizontal stripes suggests an incomplete phase transformation from 1-dH to tetragonal, perhaps due to the influence of the substrate. TEM and XRD were used to confirm the phase transformation in bulk samples.

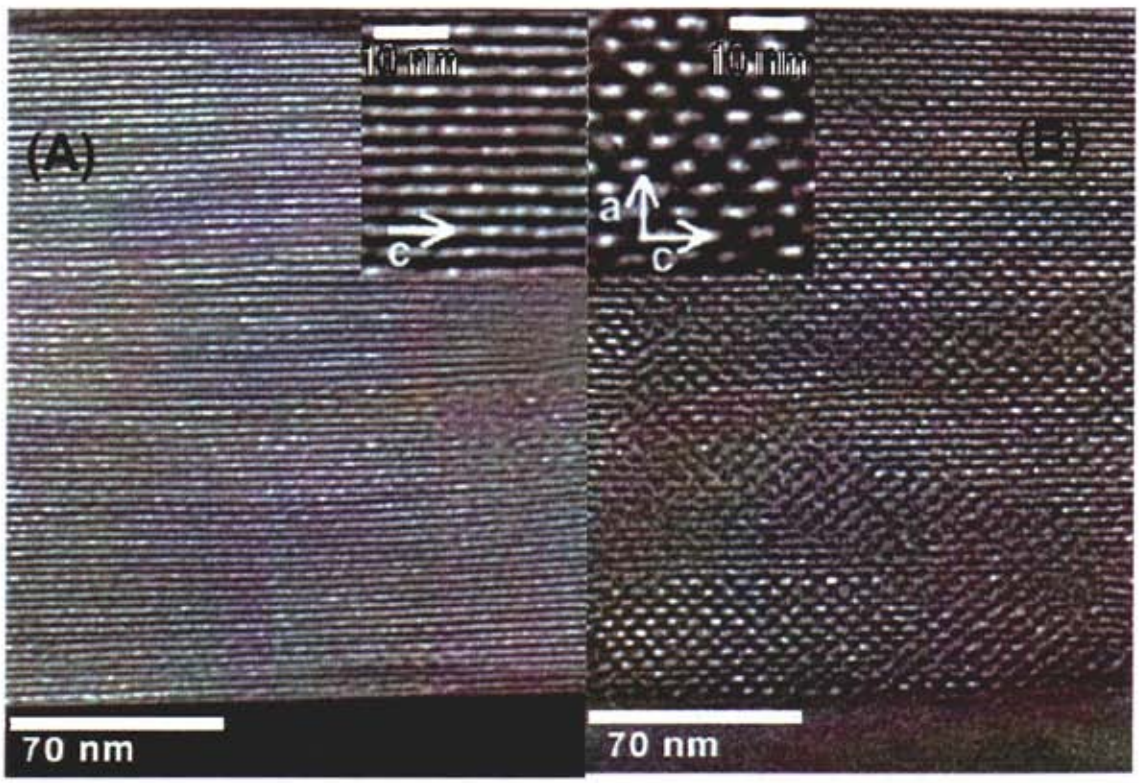

Figure 4. Cross-sectional TEM images of patterned film. (**A**) [110]-orientation of unirradiated calcined region prepared as in Fig 3 trace A. Striped pattern is consistent with 1-dH mesophase with a = 37 Å. (**B**) Irradiated calcined region prepared as in Fig 3 trace B capturing the 1-dH → tetragonal mesophase transformation. Inset: magnified image showing relationship between the 1-dH and tetragonal mesophases and defining the a and c lattice constants of the transformed tetragonal mesophase.

In our investigations, condensation of the silica framework substantially increases its acidity as reflected by a reduced pKa and isoelectric point [6]. Therefore, although the overall pH of the system is reduced by photo-induced acid generation, the protonation of the silica framework decreases relative to that of the ethylene oxide headgroups. In order to maintain charge density matching at the silica-surfactant interface, the optimal ethylene oxide headgroup area a_o must increase. The increased value of a_o in turn reduces the surfactant packing parameter g, favoring transformation to a higher curvature mesophase. This transformation to a lower density mesophase is no doubt aided by the condensation-induced tensile stress, which in effect stretches the film fostering its transformation to a lower density form.

Mechanistically, we propose the phase transformation proceeds through creation of periodic undulations along the length of the close-packed cylindrical channels of the 1-dH mesophase, as is known for the temperature-induced hexagonal-to-body-centered-cubic transformation of $C_{12}EO_{12}$ in the $C_{12}EO_{12}/H_2O$ binary system [21]. For the silica-

surfactant system, undulation results in a tetragonal (distorted cubic) packing as depicted in Fig. 5. d_{100} for the parent 1-dH mesophase becomes d_{200} of the tetragonal mesophase, resulting in a factor of $\sqrt{3}$ increase in the lattice parameter. Distortion arises due to shrinkage normal to the substrate. The phase transformation from 1-dH to tetragonal occurs with minimal displacement of the silica oligomers and surfactant species, and we expect a precise topotactic relationship between the hexagonal and tetragonal mesophases as shown schematically in Fig.5 and by TEM in Figs. 4A and 4B. There are two previous reports of condensation-driven transformations to higher curvature mesophases: lamellar to 1-dH [19] and lamellar to cubic [9], but our study appears to be the first report of a hexagonal-to-cubic or tetragonal transformation. Since it depends critically on the initial surfactant and acid concentrations, the transformation may be realized or avoided (scheme 3 versus scheme 2 of Fig. 1) by judicious choice of these parameters. In an initial study of the effects of surfactant and acid concentration on mesophase development, we observed samples prepared with 2-3 wt% Brij-56 surfactant and without PAG to exhibit a 1-dH mesophase after deposition and after calcination. Samples prepared with 3wt% Brij-56, but with a higher acid concentration exhibited a 1-dH to tetragonal transformation upon heating. Similarly samples prepared with 4 wt% Brij-56 and without PAG exhibited a 1-dH to tetragonal transformation upon heating. Through introduction of PAG followed by UV irradiation and heating we are able to realize the 1-dH to tetragonal transformation for the 3 wt% Brij-56 specimen.

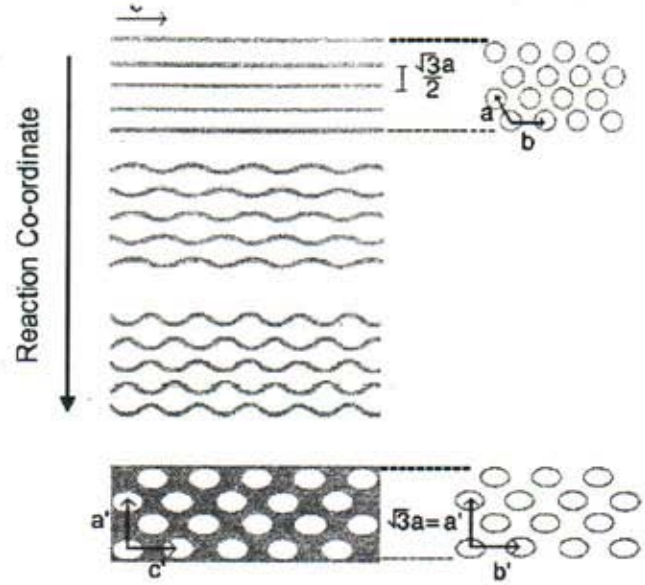

Figure 5. Schematic diagram showing the mechanism of the transformation from the 1-dH mesophase (top) to a tetragonal (distorted cubic) mesophase (bottom). As condensation of the siloxane framework proceeds, the framework charge density decreases relative to that of the EO headgroups. The corresponding increase in the optimal surfactant headgroup area drives the 1-dH to tetragonal mesophase transformation through a periodically undulating intermediate as known for the thermally driven 1-dH → body-centered-cubic transformation of of $C_{12}EO_{12}$ in the $C_{12}EO_{12}/H_2O$ binary system[21]

Conclusions

Although optical patterning of average properties, like density, of disordered, sol-gel films has been reported previously [15,16,22] the uniform initial pore size of our photosensitive thin-film mesophases combined with the UV-dose dependence of our patterning procedure provide a unique ability to adjust precisely and to define spatially the pore size along with refractive index and surface area via grayscale lithography. The observed hexagonal to tetragonal phase transformation further allows patterning of pore connectivity. These features are of practical importance for applications like membranes and microfluidic systems.

References

1. C. T. Kresge, M. E. Leonowicz, W. J. Roth, J. C. Vartuli, J. S. Beck, *Nature* **359**, 710-712 (1992).
2. Y. N. Xia, G. M. Whitesides, *Annual Review of Materials Science* **28**, 153-184 (1998).
3. P. D. Yang, et al., *Science* **282**, 2244-2246 (1998).
4. M. Trau, et al., *Nature* **390**, 674-676 (1997).
5. H. Y. Fan, et al., *Nature* **405**, 56-60 (2000).
6. C. J. Brinker, G. W. Scherer, *Sol-Gel Science* (Academic Press, San Diego, 1990), pp. 139-142.
7. C. J. Brinker, et al., *Access in Nanoporous Materials*. T. J. Pinnavaia, M. F. Thorpe, Eds. (Plenum, New York, 1995), pp. 123-139.
8. C. J. Brinker, Y. F. Lu, A. Sellinger, H. Y. Fan, *Advanced Materials* **11**, 579-585 (1999).
9. Y. F. Lu, et al., *Nature* **389**, 364-368 (1997).
10. J. V. Crivello, J. H. W. Lam, *Macromolecules* **10**, 1307-1315 (1977).
11. R. D. Miller, *Science* **286**, 421-423 (1999).

12. J. Samuel, C. J. Brinker, L. J. D. Frink, F. van Swol, *Langmuir* **14**, 2602-2605 (1998).
13. M. Lu, C. J. Brinker, *Materials Research Society Symposium Proceedings, Boston, MA,* **594** (1999).
14. K. Simmons-Potter, B. Potter, M. Sinclair, *Japanese Journal of Applied Physics Part 1-Regular Papers Short Notes & Review Papers* **37**, 8-11 (1998).
15. D. Blanc, S. Pelissier, K. Saravanamuttu, S. I. Najafi, M. P. Andrews, *Advanced Materials* **11**, 1508-& (1999).
16. Y. Moreau, et al., *Optical Engineering* **37**, 1130-1135 (1998).
17. V. K. Gupta, N. L. Abbott, *Science* **276**, 1533-1536 (1997).
18. J. Israelachvili, *Intermolecular and Surface Forces* (Academic Press, 1992), pp. 341-389.
19. J. N. Israelachvili, D. J. Mitchell, B. W. Ninham, *J. Chem. Soc.* **2**, 1525-1568 (1976).
20. A. Monnier, et al., *Science* **261**, 1299-1303 (1993).
21. P. Sakya, J. M. Seddon, R. H. Templer, R. J. Mirkin, G. J. T. Tiddy, *Langmuir* **13**, 3706-3714 (1997).
22. P. Coudray, J. Chisham, M. P. Andrews, S. I. Najafi, *Optical Engineering* **36**, 1234-1240 (1997).
23. G. C. Frye, A. J. Ricco, S. J. Martin, C. J. Brinker, *Materials Research Society Symposium Proceedings* **121**, 349-354 (1988).

Appendix A

Supplementary Figures

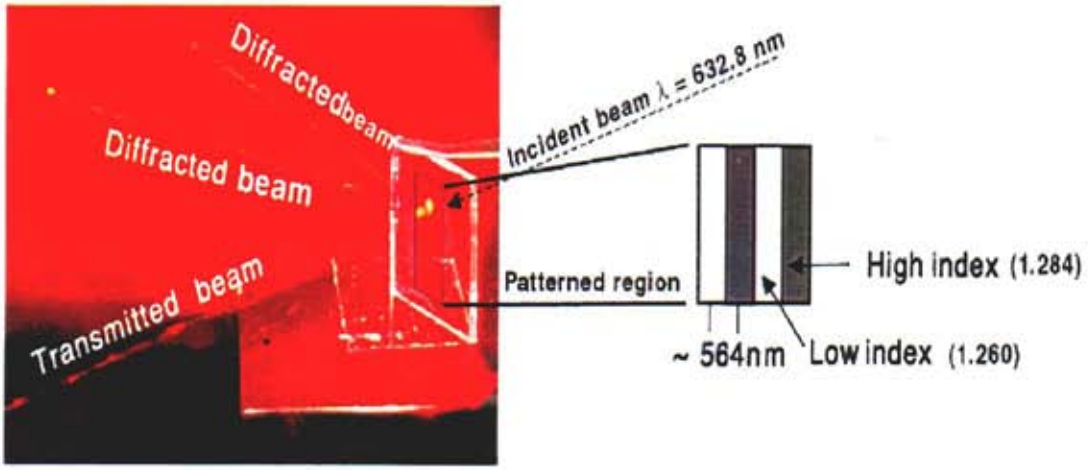

Supplemental Figure 1. Diffraction of a helium-neon laser beam into the transmission and reflected first diffracted orders from an index grating written into a photosensitive thin-film mesophase. The incident beam travels from right to left in the picture, and the diffracted orders are incident upon a white card in the background. The red coloration of the white card results from light scattering.

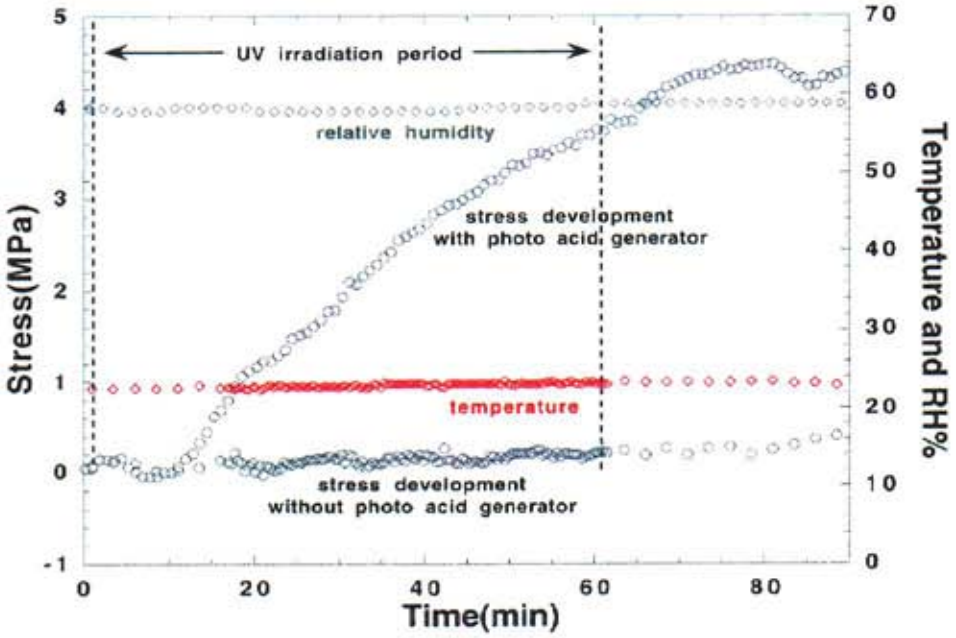

Supplemental Figure 2. Stress development during UV irradiation for films prepared with and without PAG. Development of 4.5 MPa of biaxial tensile stress is observed for films with PAG after UV irradiation of 60 min, whereas negligible stress develops for films prepared without PAG under similar conditions.

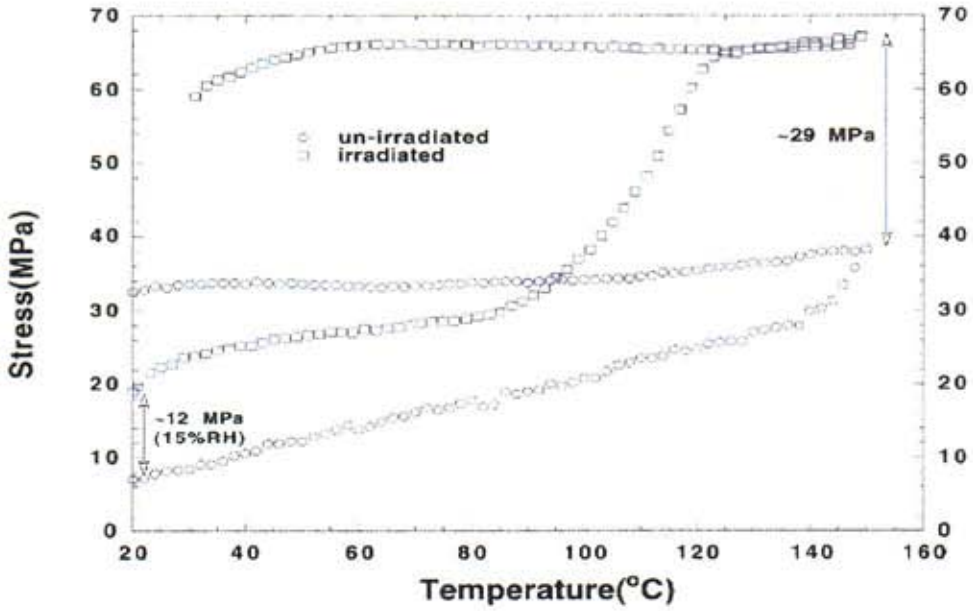

Supplemental Figure 3. Biaxial tensile stress development during the initial stage of calcination for irradiated and unirradiated films prepared with PAG measured on a Tencor FLX-2908. The irradiated film shows a higher initial stress at room temperature due to acid-promoted siloxane condensation. When heated to 150°C, the irradiated film develops an additional 48 MPa of stress, whereas the unirradiated film develops an additional 30 MPa.

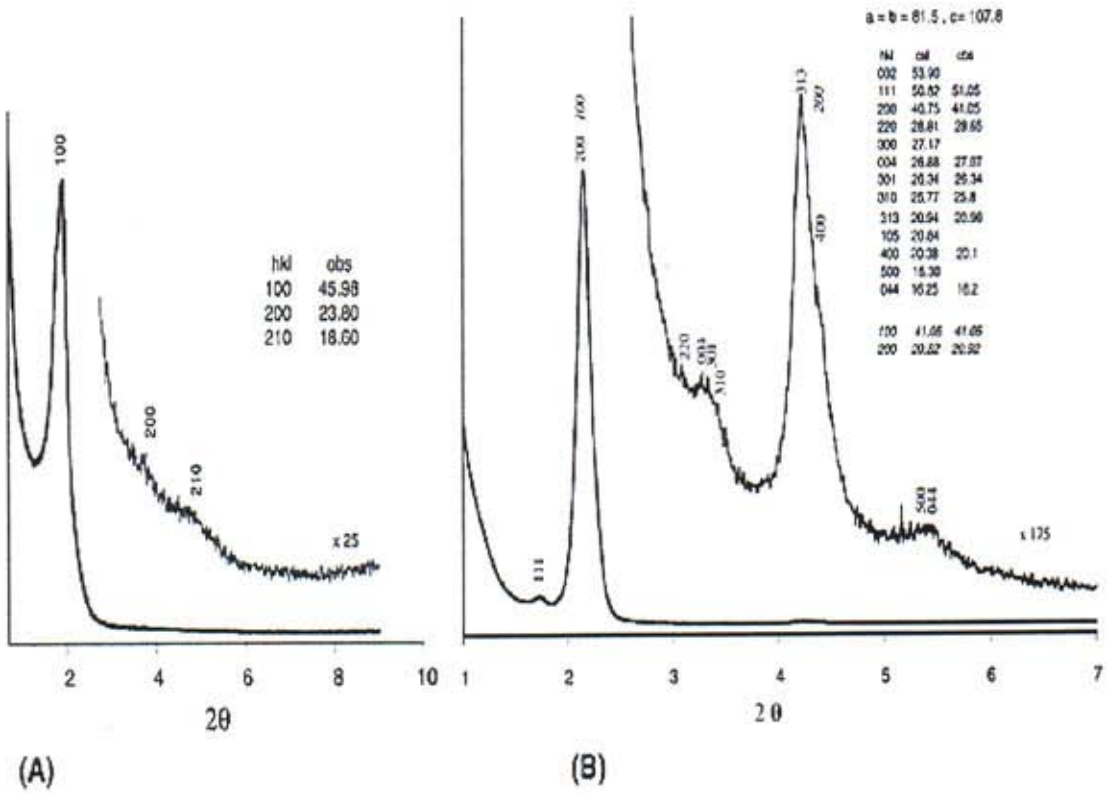

Supplemental Figure 4. Powder X-ray diffraction pattern for calcined silica/surfactant mesophases. (A) The pattern for the unirradiated powder is consistent with a 1-dH mesostructure with lattice constant a = 52.8 Å. The high 2θ region is magnified by 25. (B) The pattern for UV-irradiated powder is consistent with tetragonal mesophase with a = b = 81.5 Å, c = 107.8 Å. The high 2θ region is magnified by 175. Note that the (200) and (400) reflections of the tetragonal mesophase could also be indexed as (100) and (200) reflections of a 1-dH mesophase with a = 47.4 Å

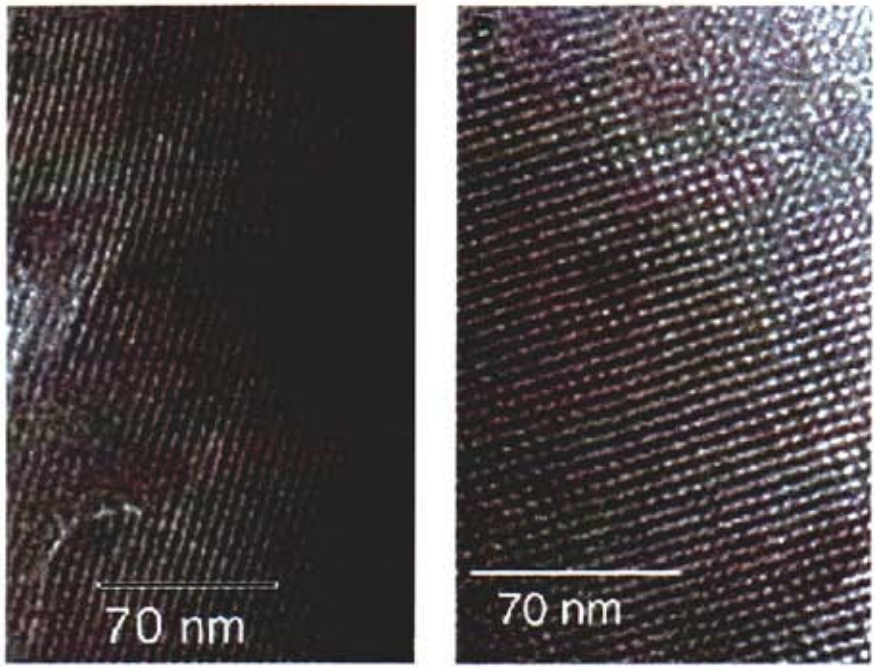

Supplemental Figure 5. TEM images of calcined powder samples. (A) Unirradiated powder corresponding to the [110] orientation of a 1-dH mesophase. (B) UV-irradiated powder corresponding to the [001] orientation of a tetragonal mesophase.

DISTRIBUTION:

1 Mr. Dhaval Doshi
University of New Mexico
Advanced Materials Laboratory
1001 University Blvd. SE
Albuquerque, NM 87106

1 Dr. Mengcheng Lu
Intel Corporation / RAI-234
5200 N.E. Elan Young Parkway
Hillsboro, OR 97124

1 Dr. Yunfeng Lu
Tulane University
Chemical Engineering Dept.
New Orleans, LA 70005

1 Dr. Nicola Husing
Getreidemarkt 9 / E-153
Institute of Inorganic Chemistry
Tuvienna A-1060 Vienna
Austria / Europe

1 Dr. Alan Hurd
Los Alamos National Laboratory
MS H805 LNNSCE-12: Lujan Center
Los Alamos, NM 87545

1	MS 1349	C. Ashley
6	MS 1349	C. Jeffrey Brinker
1	MS 1349	N. B. Jackson
1	MS 1411	K. Simmons-Potter
1	MS 1411	B.G. Potter
1	MS 9018	Central Technical Files, 8940-2
2	MS 0899	Technical Library, 4916
1	MS 0612	Review and Approval Desk, 15102 For DOE/OSTI
1	MS 0161	Patent and Licensing Office, 11500